

# Constraints to Dark Matter from Inert Higgs Doublet Model

Marco Aurelio Díaz, Benjamin Koch, and Sebastián Urrutia-Quiroga\*

*Instituto de Física, Pontificia Universidad Católica de Chile, Av. Vicuña Mackenna 4860, Santiago, Chile*

\*sgurruti@uc.cl

We study the Inert Higgs Doublet Model and its inert scalar Higgs  $H$  as the only source for dark matter. It is found that three mass regions of the inert scalar Higgs can give the correct dark matter relic density. The low mass region (between 3 and 50 GeV) is ruled out. New direct dark matter detection experiments will probe the intermediate (between 60 and 100 GeV) and high (heavier than 550 GeV) mass regions. Collider experiments are advised to search for  $D^\pm \rightarrow HW^\pm$  decay in the two jets plus missing energy channel.

## I. INTRODUCTION

Astrophysical observations provide strong evidence for the existence of Dark Matter (DM) [1], and its abundance in the current phase of the Universe [2]. According to the newest results from Planck collaboration, there is a 74% approximately of matter which is not directly visible but is observed due to its gravitational effects on visible matter. Additional evidence for the existence of DM comes from study the rotation curves of spiral galaxies [3], the analysis of the bullet cluster [4], and the study of baryon acoustic oscillations [5]. One of the most common hypothesis used to explain these phenomena is to postulate the existence of weakly interacting massive particles (WIMPs) [6].

In order to explain DM, we study a simple extension of the Standard Model (SM), called the Inert Higgs Doublet Model (IHDM). This model, which was originally proposed for studies on electroweak (EW) symmetry breaking [10], introduces an additional doublet and a discrete symmetry. These two characteristics of the model modify the SM phenomenology, but there are some regions of the parameter space which predict only small deviations from the SM. Nevertheless, one of the most attractive characteristic of the IHDM is the presence of an stable neutral particle which can be a DM candidate.

In this work the IHDM is revisited, considering various restrictions, focusing our analysis on the zones of the parameter space which reproduce the correct DM relic density according to the newest measurements [7, 8]. In this context, three not connected mass regimes for the lightest inert particle are found. These regimes are also analyzed using LHC observables like branching ratios to invisible particles and an specific SM-like

Higgs boson decay mode. Additionally, we study some inert decays modes. Finally, we use a direct detection approach to rule out one of the mass regimes. It is further shown that this regime can also be ruled out by constraints from collider physics [9].

This paper is organized as follows. After a short introduction in section I the model is introduced in section II by formulating the associated potential and constraints of the model, and by exploring the parameter space and its characteristics in section III. In section IV the behavior of the model is presented from a collider physics perspective, studying the modifications of the SM and its implications for the IHDM. In section V the results of this study are complemented by an analysis from the Dark Matter perspective. Finally, in section VI we remark on the most important conclusions of our work.

## II. THE INERT HIGGS DOUBLET MODEL

Consider an extension of Standard Model (SM), which contains two Higgs doublets  $\Phi_{S,D}$  and a discrete  $\mathbb{Z}_2$  symmetry [10] ( $\Phi_S \xrightarrow{\mathbb{Z}_2} \Phi_S$  and  $\Phi_D \xrightarrow{\mathbb{Z}_2} -\Phi_D$ ). All fields of the SM are invariants under the discrete symmetry, and  $\Phi_S$  is completely analogous to the SM Higgs doublet.

The most general renormalizable  $SU(2) \times U(1)$  invariant Higgs potential, that also preserves the discrete symmetry is,

$$V = \mu_1^2 \mathbf{A} + \mu_2^2 \mathbf{B} + \lambda_1 \mathbf{A}^2 + \lambda_2 \mathbf{B}^2 + \lambda_3 \mathbf{A} \mathbf{B} + \lambda_4 \mathbf{C}^\dagger \mathbf{C} + \frac{\lambda_5}{2} (\mathbf{C}^2 + \mathbf{C}^{\dagger 2}) \quad , \quad (1)$$

where  $\mathbf{A}, \mathbf{B}, \mathbf{C}$  are given by,

$$\mathbf{A} = \Phi_S^\dagger \Phi_S, \quad \mathbf{B} = \Phi_D^\dagger \Phi_D, \quad \mathbf{C} = \Phi_S^\dagger \Phi_D \quad . \quad (2)$$

The parameters  $\mu_i^2$  ( $i = 1, 2$ ) and  $\lambda_j$  ( $j = 1 \dots 4$ ) are intrinsically real, and  $\lambda_5$  will be assumed to be real [11]. After Spontaneous Symmetry Breaking, the vacuum expectation values of the Higgs doublets are,

$$\langle \Phi_S \rangle = \frac{1}{\sqrt{2}} \begin{pmatrix} 0 \\ v \end{pmatrix}, \quad \langle \Phi_D \rangle = \begin{pmatrix} 0 \\ 0 \end{pmatrix} \quad , \quad (3)$$

where  $\langle \Phi_D \rangle$  is forced by the discrete symmetry, and  $v = 246$  GeV. Expanding the fields around those vacua, we define,

$$\Phi_S = \begin{pmatrix} G^+ \\ (v + h + iG^0)/\sqrt{2} \end{pmatrix}, \quad \Phi_D = \begin{pmatrix} D^+ \\ (H + iA)/\sqrt{2} \end{pmatrix} \quad , \quad (4)$$

where  $G^0$  and  $G^\pm$  are the neutral and charged Goldstone bosons, and  $h$  is the SM-like Higgs boson. The fields in the second doublet belong to the so called “*dark*” or “*inert*” sector. They are the scalar  $H$  and pseudoscalar  $A$ , both neutral, and the charged scalar  $D^\pm$ . As in the SM, the parameter  $\mu_1^2$  is related to  $\lambda_1$  by the tree-level tadpole condition  $\mu_1^2 = -\lambda_1 v^2$ . The masses of physical states [12, 13] are,

$$\begin{aligned} m_h^2 &= 2\lambda_1 v^2 \quad , \\ m_D^2 &= \mu_2^2 + \frac{\lambda_3}{2} v^2 \quad , \\ m_H^2 &= m_D^2 + \left( \frac{\lambda_4 + \lambda_5}{2} \right) v^2 = \mu_2^2 + \frac{\lambda_{345}}{2} v^2 \quad , \\ m_A^2 &= m_D^2 + \left( \frac{\lambda_4 - \lambda_5}{2} \right) v^2 \quad , \end{aligned} \quad (5)$$

with

$$\lambda_{345} = \lambda_3 + \lambda_4 + \lambda_5 \quad . \quad (6)$$

As independent and free parameters we take the masses  $m_H$ ,  $m_A$ , and  $m_D$  at tree-level, and the couplings  $\lambda_2$  and  $\lambda_{345}$ . The SM-like Higgs boson mass is fixed now thanks to the measurement  $m_h = 125$  GeV [14, 15].

The constraints we initially impose includes vacuum stability at tree-level, where constraints on the  $\lambda_i$  couplings and  $\mu_i$  mass terms appear [16–18]; perturbativity ( $|\lambda_i| < 8\pi$ ) [19, 20] and unitarity [21], where we impose that the scalar potential is unitary and that several scattering processes between scalar and gauge bosons are bounded; electroweak precision tests through the  $S$ ,  $T$ , and  $U$  parameters [22] applied to the IHDM [21, 23], with  $3\sigma$  values given by

$$S \Big|_{U=0} = 0.06 \pm 0.09 \quad \wedge \quad T \Big|_{U=0} = 0.10 \pm 0.07 \quad , \quad (7)$$

with a correlation coefficient of +0.91 [24] and collider constraints [16, 25–27], where we satisfy lower bounds on the Higgs boson masses.

The DM particle must be neutral. In our analysis we assume it is the  $H$  boson, thus  $m_H < m_A$  and  $m_H < m_D$ , which due to (5) translates to

$$\lambda_4 + \lambda_5 < 0 \quad \wedge \quad \lambda_5 < 0 \quad . \quad (8)$$

We do not consider  $A$  as the DM candidate because it is analogous to consider  $H$  as the DM candidate defining  $\lambda_{345}^- = \lambda_3 + \lambda_4 - \lambda_5$  instead of  $\lambda_{345}$ .

### III. IHDM PARAMETER SPACE

We randomly scan the parameter space of the IHDM, taking into account all the constraints mentioned in the previous section. Additionally, we compute some astrophysical properties of the model using the `micrOMEGAS` software [28]. We consider masses satisfying  $1 \text{ GeV} < m_i < 1 \text{ TeV}$ , where  $i = H, A, D$ . In addition, we consider cosmological measurements: the DM relic density  $\Omega_{DM} h^2$  is a property related to its abundance in the current phase of the Universe. This quantity is well measured by WMAP [29] and Planck [30] experiments. Following [31] to combine both measurements we obtain,

$$\Omega_{DM} h^2 = 0.1181 \pm 0.0012 \quad . \quad (9)$$

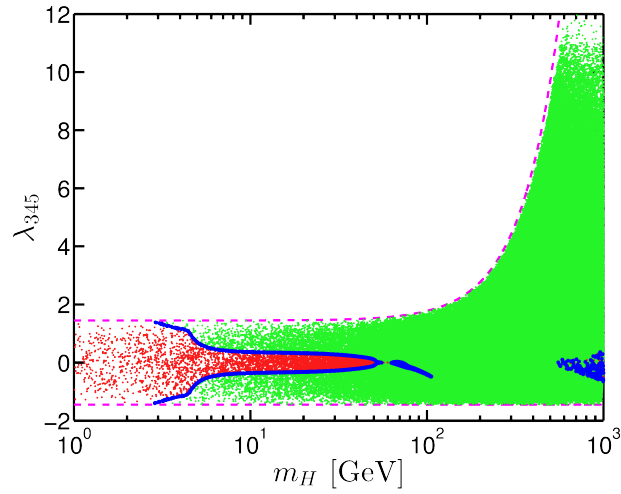


FIG. 1: Random scan of IHDM parameter space. Coupling  $\lambda_{345}$  as a function of the DM candidate mass  $m_H$ . The upper dotted line is the bound generated by the inert vacuum condition and the lower dotted line is generated by the vacuum stability condition.

In Figure 1 the coupling  $\lambda_{345}$ , is shown as a function of the Higgs boson mass  $m_H$  varying ( $\mu_i, \lambda_i, m_A, m_D$  and  $m_H$ ). We work with the hypothesis that the light inert Higgs boson  $H$  is providing the complete DM density  $\Omega_{DM} h^2$  given in (9). The color code is as follows: red points (dark gray) produce a relic density above the  $3\sigma$  limit given in eq. (9); blue points (black) produce a relic density within the  $3\sigma$  region; green points (light gray) produce a relic density below the  $3\sigma$  limit. Regarding the points that satisfy the relic density we see three clear regions [12, 32], one for low  $m_H$  ( $3 < m_H < 50 \text{ GeV}$ ), another one for medium  $m_H$  ( $60 < m_H < 100 \text{ GeV}$ ) and finally one for high values of  $m_H$  ( $m_H > 550 \text{ GeV}$ ). The explanation for the

gap is related to annihilation processes and it will be given later. At  $m_H < 3$  GeV the IHDM can no longer be compatible with vacuum existence and stability [33, 34].

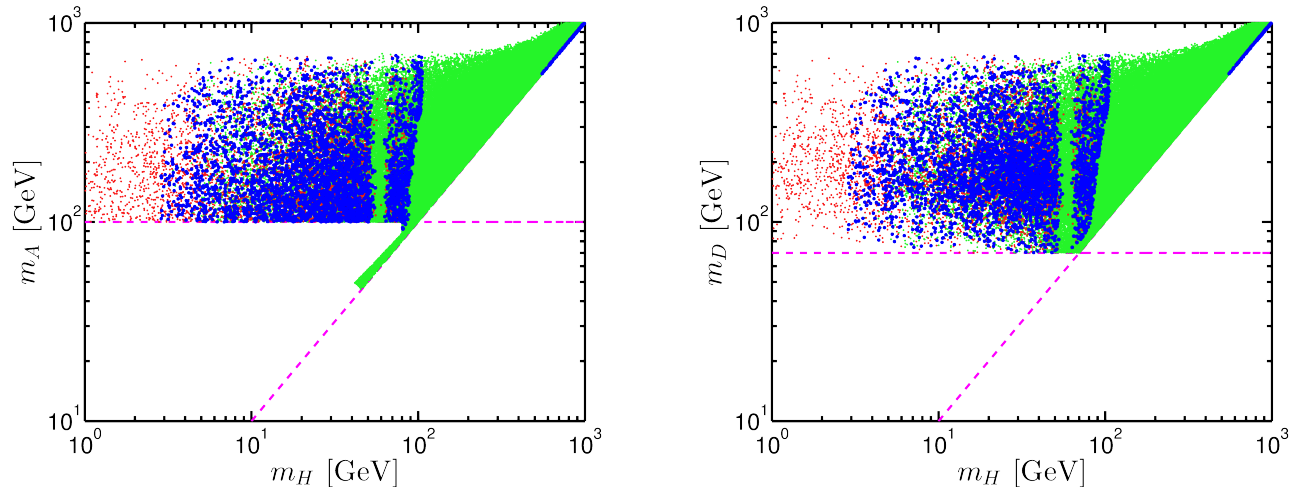


FIG. 2: Inert Higgs masses  $m_A$  (left panel) and  $m_D$  (right panel) as a function of the DM candidate mass  $m_H$ , for the same random scan of IHDM parameter space. The horizontal dotted line is due to LEP constraints and the diagonal dotted line is due to the  $m_H$ -DM condition.

In Fig. 2 we have for the same scan and color code the mass of the heavy pseudoscalar  $m_A$  (left) and the mass of the charged Higgs  $m_D$  (right) as a function of the mass of the DM candidate  $m_H$ . Due to dedicated pre-LHC collider searches, a bound that captures most of the features is  $m_A > 100$  GeV and  $m_D > 70$  GeV. This is so with the exception of a small strip for  $m_A < 100$  GeV seen in the left panel of Fig. 2, where due to the proximity of the  $H$  and  $A$  masses the search loses sensitivity. In this figure the gap in values of  $m_H$  when the relic density is imposed is apparent. Notice that the density of solutions is larger when the masses for  $H$ ,  $A$ , and  $D$  are close to each other, and that this feature is more pronounced when the masses of these particles are near the TeV scale (due to the logarithmic scale). Finally we notice that  $\Omega_{DM} h^2$  is more sensible to the parameters  $\lambda_{345}$  and  $m_H$  (Fig. 1) than the masses of the other inert particles (Fig. 2).

#### IV. COLLIDER PHYSICS

As we mentioned before, the Higgs boson discovered at CERN in 2012 is the SM-like Higgs boson  $h$  of our model from the non-inert Higgs doublet field  $\Phi_S$ . This particle  $h$  couples to the charged Higgs pair ( $D^\pm$ ),

which contributes to the diphoton decay width<sup>1</sup>  $\Gamma(h \rightarrow \gamma\gamma)$  [35]. For the same reason  $D^\pm$  also contribute to  $\Gamma(h \rightarrow Z\gamma)$ .

It is convenient to work with the parameter [21, 34, 38]

$$R_{\gamma\gamma} = \frac{B(h \rightarrow \gamma\gamma)^{IHDM}}{B(h \rightarrow \gamma\gamma)^{SM}} . \quad (10)$$

The value we use for the SM is  $\Gamma(h_{SM} \rightarrow \gamma\gamma) = 4.1$  MeV [39]. ATLAS [40] and CMS [41] collaborations have studied this decay mode, and if we combined both results [31] obtain  $R_{\gamma\gamma}^{exp} = 1.14 \pm 0.18$ .

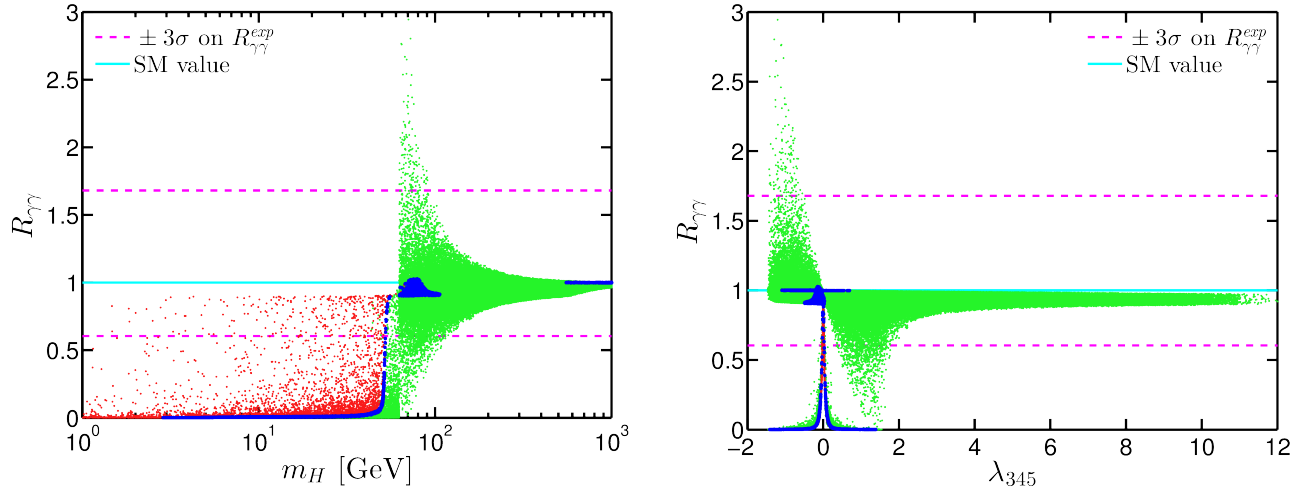


FIG. 3:  $R_{\gamma\gamma}$  parameter as a function of the DM candidate mass  $m_H$  (left panel) and the  $\lambda_{345}$  coupling (right panel), for the same random scan of IHDM parameter space.

In Fig. 3 we have the parameter  $R_{\gamma\gamma}$  as a function of the DM candidate mass  $m_H$  (left panel) and as a function of the coupling  $\lambda_{345}$  (right panel). The points in parameter space that produce a correct relic density can be divided in three groups. In the case of very light masses for the DM candidate ( $3 < m_H < 50$  GeV approximately) the decay mode  $h \rightarrow HH$  is open, and  $R_{\gamma\gamma}$  is close to zero ruling those masses out [42]. In the intermediate mass case, approximately between 60 and 100 GeV, there is a region with acceptable solutions characterized by  $R_{\gamma\gamma} \approx 1$ . This region is characterized by increasingly heavier values for  $A$  and  $D^\pm$ . In the large mass region ( $m_H > 550$  GeV approximately), the charged Higgs  $D^\pm$  gives a negligible contribution to the decay  $h \rightarrow \gamma\gamma$  such that  $R_{\gamma\gamma}$  is close to unity. Interestingly, the right panel of Fig. 3 shows that perturbative values ( $|\lambda_{345}| < 1$ ) are preferred.

<sup>1</sup> In this scenario, the IHDM cannot reproduce the reported excess of diphoton events by ATLAS [36] and CMS [37] Collaborations in their Run-II 13 TeV analyses, because the  $\mathbb{Z}_2$  symmetry prevent the extra Higgs bosons of the model from decaying into two photons.

In addition, if the inert particles are light enough, there are two other two-body decays which are:

$$\begin{aligned}\Gamma(h \rightarrow HH) &= \frac{v^2 \lambda_{345}^2}{32\pi m_h} \sqrt{1 - \frac{4m_H^2}{m_h^2}} \quad , \\ \Gamma(h \rightarrow AA) &= \frac{\left(m_A^2 - m_H^2 + \lambda_{345} v^2/2\right)^2}{8\pi v^2 m_h} \sqrt{1 - \frac{4m_A^2}{m_h^2}} \quad .\end{aligned}\tag{11}$$

There is no phase space for a two-body decay  $h \rightarrow D^\pm D^\mp$ . It is possible to define the parameter  $R_{Z\gamma}$ , in analogy to  $R_{\gamma\gamma}$  defined in eq. (10). It is interesting that even though the decay  $h \rightarrow Z\gamma$  is not well measured, it still can give additional insight to the model [43, 44]. As Fig. 4 shows, there appears a very narrow correlation between  $R_{\gamma\gamma}$  and  $R_{Z\gamma}$ , which is a common feature for  $R_{\gamma\gamma}$  v/s  $R_{Z\gamma}$  plots [17, 18, 45]. The bisector branch

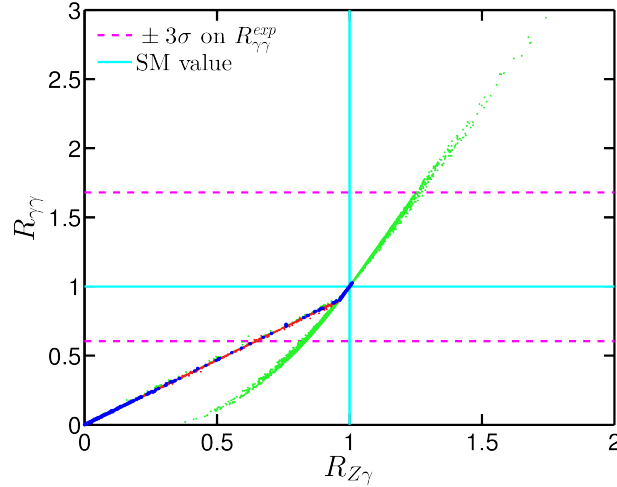


FIG. 4: Relation between  $R_{\gamma\gamma}$  and  $R_{Z\gamma}$  for the same random scan of IHDM parameter space.

only contains points that satisfy  $m_H < m_h/2$  (inert invisible decay channel open). Points of parameter space which satisfy the relic density and have low DM candidate mass are ruled out, because they produce a too small value for  $R_{\gamma\gamma}$ . By analyzing the characteristics of the those data points one finds that the larger branch includes only points with  $m_H > m_h/2$ , and the ones that also satisfy relic density are close to  $R_{\gamma\gamma} = R_{Z\gamma} = 1$ , as it was mentioned before. The two branches seen in the  $R_{\gamma\gamma}$  v/s  $R_{Z\gamma}$  relation also appear in the non-normalized  $B(h \rightarrow \gamma\gamma)$  v/s  $B(h \rightarrow Z\gamma)$  relation (not shown). But it is reduced only to the long (green) branch in the  $\Gamma(h \rightarrow \gamma\gamma)$  v/s  $\Gamma(h \rightarrow Z\gamma)$  relation. Further one sees that when the  $h \rightarrow HH$  decay channel is closed, the  $D^\pm$  loop transforms into the long branch the otherwise SM dot (the intersection point between the two branches). If the  $h \rightarrow HH$  decay channel is open, the second branch appears because the  $h \rightarrow HH$  channel tends to dominate [46].

We are also interested in the invisible decay of the SM-like Higgs boson. If the DM candidate mass satisfy  $m_H < m_h/2$ , the two-body decay channel  $h \rightarrow HH$  is open, which is invisible for the LHC detectors, and shows only as missing momentum. There are measurements for the invisible decay of the SM-like Higgs from the LHC experiments. Taking a simple average of the upper bounds to the invisible decay rate from ATLAS [47] and CMS [48], gives  $B(h \rightarrow \text{inv}) < 0.43$  for the SM-like Higgs boson. In Fig. 5 we show the branching

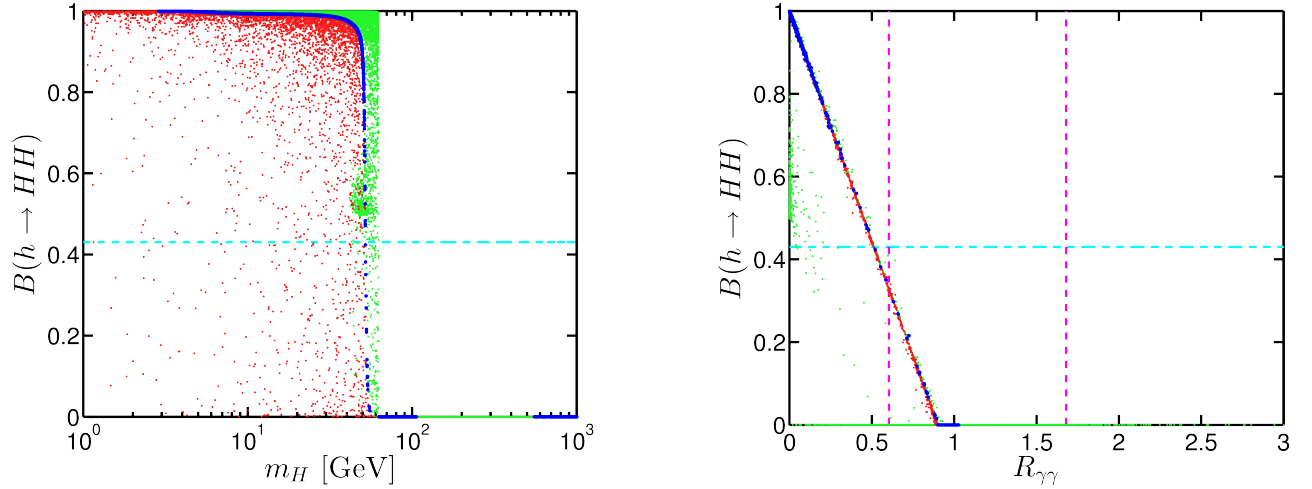


FIG. 5: Branching ratio for the invisible decay of the SM-like Higgs boson as a function of the DM candidate mass  $m_H$  (left panel) and as a function of the parameter  $R_{\gamma\gamma}$  (right panel), for the same random scan of IHDM parameter space. Please note that there is a number of points on the  $m_H$  and  $R_{\gamma\gamma}$  axes, with  $B(h \rightarrow HH) = 0$ .

ratio for the invisible decay of the SM-like Higgs boson  $B(h \rightarrow HH)$ , as a function of the mass of the DM candidate  $m_H$  (left panel) and as a function of the parameter  $R_{\gamma\gamma}$  (right panel). In the left panel we also have a horizontal line that shows the upper bound for  $B(h \rightarrow HH)$  mentioned above. The threshold  $2m_H = m_h$  appears clearly in the left panel. Most of the points with correct relic density satisfying  $m_H < 60$  GeV are ruled out because they produce a too large invisible branching ratio for  $h$ . On the contrary, most of the points with higher DM candidate mass are fine because they produce an invisible branching ratio equal to zero. In the right panel, where we have as dashed lines the bounds from LHC experiments, we see a very strong relation between  $B(h \rightarrow HH)$  and  $R_{\gamma\gamma}$ . The points that satisfy relic density with a low mass for the DM candidate are simultaneously excluded from  $B(h \rightarrow HH)$  and from  $R_{\gamma\gamma}$ . The rest of the points satisfy the bounds.

To finalize this section we discuss the branching ratios for the two observable inert Higgs bosons  $A$  and  $D^\pm$ . In Fig. 6 we have the branching ratios for the pseudoscalar Higgs boson (left panel) as a function of its mass, and the branching ratios for the charged Higgs boson (right panel) as a function of its mass. In



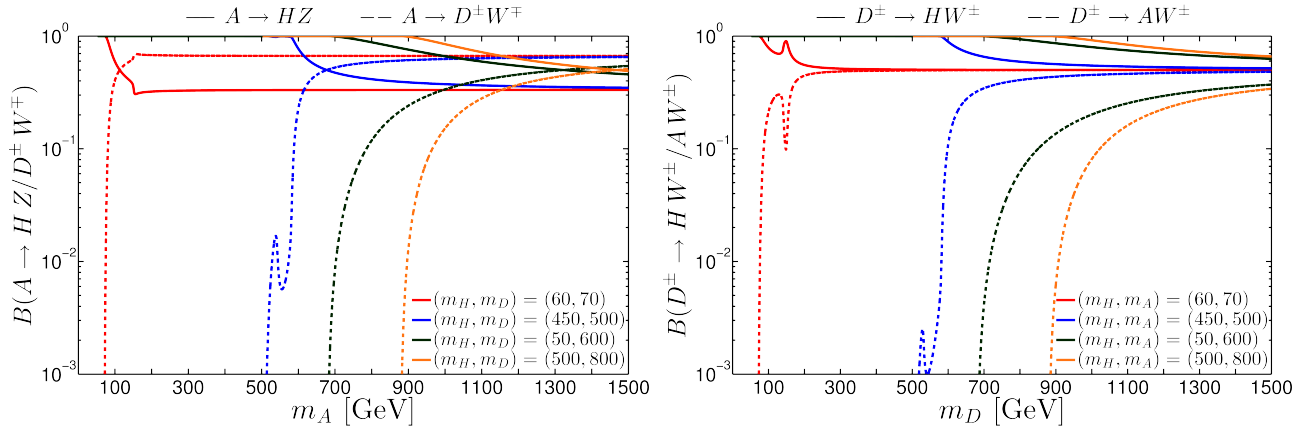


FIG. 6: Branching ratios for the inert Higgs bosons  $A$  (left panel) and  $D^\pm$  (right panel) as a function of their corresponding mass.

the left panel we show the decays of the inert pseudoscalar Higgs  $A$ , which are  $A \rightarrow HZ$  (solid line) and  $A \rightarrow D^\pm W^\mp$  (dashed line). As it can be seen from the Feynman rules, the only unknown parameters the branching ratios depend on are the masses  $m_H$ ,  $m_A$ , and  $m_D$ . Therefore, four scenarios are considered: (i)  $(m_H, m_D) = (60, 70)$ , (ii)  $(450, 500)$ , (iii)  $(50, 600)$ , and (iv)  $(500, 800)$  GeV. The gauge boson can be off-shell, although we consider the inert Higgs bosons always on-shell. The oscillation near the threshold is due to different increasing rates for the decay rates when the gauge boson is off-shell. The branching ratio  $B(A \rightarrow HZ)$  is always large (because  $m_H < m_D$ ) while  $B(A \rightarrow D^\pm W^\mp)$  can be low near thresholds. There is a crossing point where  $B(A \rightarrow HZ) = B(A \rightarrow D^\pm W^\mp)$ . In the right panel we show the decays of the charged Higgs  $D^\pm$ . Analogous scenarios are considered, but replacing  $m_D$  by  $m_A$ . In solid line we have the branching ratio for the decay  $D^\pm \rightarrow HW^\pm$  and in dash we have  $D^\pm \rightarrow AW^\pm$ . In the case of  $D^\pm$ , there is no crossing point, thus  $B(D^\pm \rightarrow HW^\pm)$  is always larger than  $B(D^\pm \rightarrow AW^\pm)$ . We remind the reader that the presence of a Higgs boson  $H$  in a final state is seen as missing momentum at the LHC.

## V. COSMOLOGY AND DARK MATTER

The existence of Dark Matter seems to be well established now [49]. There are several candidates for DM, among them the previously mentioned WIMPs. A good particle candidate for DM must be neutral and stable (or quasi-stable). The  $\mathbb{Z}_2$  discrete symmetry in the model studied in this article ensures that the lightest of the inert Higgs bosons is stable. Observation implies it is either  $H$  or  $A$  (or in a fine tuned scenario both). In this article we study the former case. An important restriction this candidate must satisfy is that its mass

density must agree with experimental observations. We calculate the relic density of our DM candidate using `micrOMEGAS` software [28]. To better understand the results on the relic density, we calculate also the thermal averaged annihilation cross section times the relative velocity  $\langle\sigma v\rangle$ , or annihilation cross section for short.

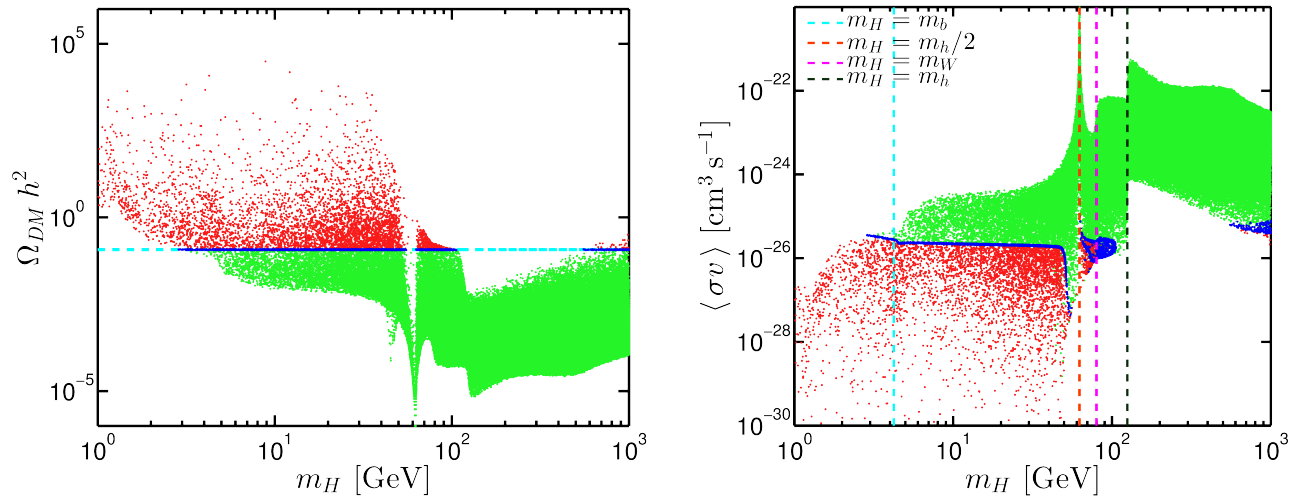


FIG. 7: Relic density for  $H$  as a function of its mass  $m_H$  (left panel), and annihilation cross section for  $H$  also as a function of its mass  $m_H$ , for the same random scan of IHDM parameter space.

In Fig. 7 we plot the  $H$  relic density as a function of the DM candidate mass  $m_H$  (left panel), and the annihilation cross section also as a function of the DM candidate mass  $m_H$  (right panel), calculated with [28]. For the relic density case, we also show, as an horizontal dashed line, the experimentally measured value for  $\Omega_{DM}h^2$  as given in eq. (9). The scan shows a large distribution with differences that can reach more than 10 orders of magnitude. For this reason most of the points in the scan are ruled out if one demands that  $H$  is actually the only WIMP responsible for the observed DM signatures. There are two mass gaps that divide the mass region in three: low mass ( $3 < m_H < 50$  GeV approximately), medium mass ( $60 < m_H < 100$  GeV approximately), and high mass ( $550 < m_H$  approximately). The origin of these mass gaps is better understood with the aid of the right frame. In the right frame of Fig. 7 we show the annihilation cross section as a function of the DM candidate mass  $m_H$ , with vertical lines denoting different thresholds. The first gap is near the threshold  $m_H \approx m_h/2$  where the annihilation channel  $HH \rightarrow h$  becomes very efficient due to the on-shellness of the SM-like Higgs  $h$ . The second gap starts at the thresholds  $m_H \approx m_W$  and  $m_H \approx m_Z$ , where  $HH \rightarrow WW(ZZ)$  become available, and continue later with the threshold  $m_H \approx m_h$  where the channel  $HH \rightarrow hh$  opens up. The annihilation channel  $HH \rightarrow t\bar{t}$  also helps. All these new annihilation channels make the DM annihilation very efficient, and it is not possible to obtain a relic density according to

observations. On the other hand, for larger  $m_H$ , it is possible to get a correct relic density if the difference between the three inert scalar masses is not so large and  $\lambda_{345}$  remains small enough [50] (see Fig. 1).

We finally study the direct detection prospects of our DM candidate. We do that through the tree-level spin-independent DM-nucleon interaction cross section [51], which applied to our case is,

$$\sigma_{DM-N}^{SI} = \frac{\lambda_{345}^2}{(4\pi m_h^4)} \frac{m_N^4 f_N^2}{(m_H + m_N)^2} . \quad (12)$$

Here  $m_h$  is the mass of the SM-like Higgs boson,  $m_H$  is the mass of the DM candidate,  $m_N$  is the nucleon mass, taken here to be  $m_N = 0.939$  GeV as the average of the proton and neutron masses,  $\lambda_{345}$  is the combined coupling defined in eq. (6), and  $f_N$  is a form factor that depends on hadronic matrix elements [52, 53].

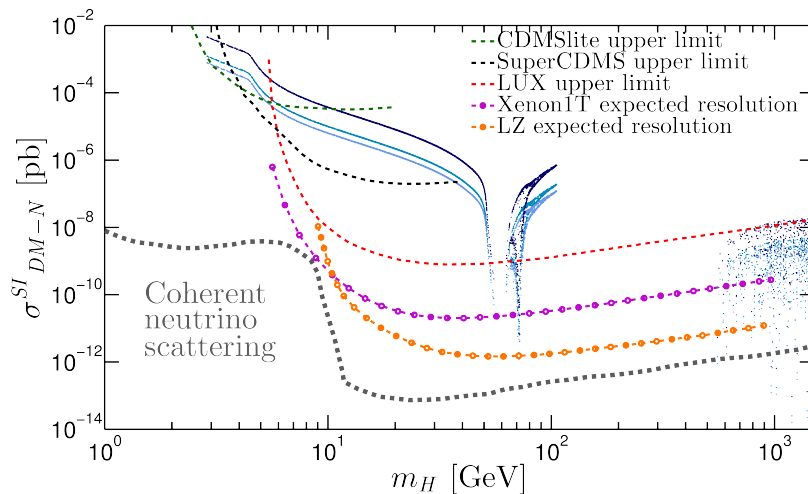


FIG. 8: *Spin-independent DM-nucleon cross section as a function of the DM candidate mass, for points of the IHDM with DM relic density consistent with observation. Three scenarios are considered with different values for the form factor  $f_N$ . Lower bounds for past experiments and prospects of measurements for future experiments are shown.*

In Fig. 8 we show the DM-nucleon cross section as a function of the DM candidate mass for a correct value of  $\Omega_{DM} h^2$ . We consider three values for  $f_N$ : a central value (0.326) from a lattice calculation [54], and extreme values (0.260 and 0.629) from the MILC collaboration [55]. Lower bounds for past experiments and prospects of measurements for future experiments are also shown [56–59]. Notice that the dispersion of points for high  $m_H$  can be understood from analogous dispersion seen in Fig. 1, and the same situation occurs with the line-like distribution for light  $m_H$ . We also show the coherent neutrino scattering upper limit [60]. This curve represents the threshold below which the detector sensitivity is such that not only the possible DM scattering effects can be observed, but also the indistinguishable scattering effects associated with neutrinos.

Thus, this indicates a region where the neutrino background becomes dominant and and little information can be obtained on DM effects. Current direct detection of DM exclude all the low DM mass points, and most of the medium DM mass points. Allowed are a narrow region near 60 GeV, and all the high mass region. Note, that the absence of points in the range of  $\sim 100 - 550$  GeV in this plot is due to the fact that the plotted points are only those that give the right dark matter density (“blue points”). Future experiments will be able to test large parts of these two regions, but will not be able to rule them out entirely if there is no signal.

## VI. CONCLUSIONS

In this article the Inert Higgs Doublet Model is studied, with the inert Higgs boson  $H$  as a DM candidate, using the latest results for DM relic density, annihilation cross section, and collider searches. As a summary we highlight,

- The branching ratios for the charged Higgs  $D^\pm$  and for the pseudoscalar Higgs  $A$  are studied and shown in Fig. 6. The  $\mathbb{Z}_2$  symmetry strongly reduces the number of different decay channels. Considering the Higgs boson on-shell and allowing the gauge boson to be off-shell (a different choice would produce different decay channels, but with smaller branching ratios), we find that  $B(D^\pm \rightarrow HW^\pm) > B(D^\pm \rightarrow AW^\pm)$  as opposed to the  $A$  decays, where there is a crossing point not far from the threshold. For this reason, in collider searches we recommend to look for a signal for a  $D^\pm$ : two jets (consistent with a  $W$ ) and missing energy (from the DM candidate  $H$ ).
- Three distinct  $H$  mass regions are found that produced the correct relic density (*i.e.*  $H$  is the only source for DM) as it can be seen in Fig. 7. The low mass region (between 3 and 50 GeV approximately) is already ruled out because it produces a too small value for  $R_{\gamma\gamma}$  (Fig. 3), because it produces a too high value for  $B(h \rightarrow HH)$  (Fig. 5), and because of direct DM searches (Fig. 8). The intermediate mass region (between 60 and 100 GeV approximately) and the high mass region (heavier than 550 GeV approximately) are allowed.
- In Fig. 8 we study the DM candidate direct detection. The low mass region is also ruled out by present experiments. In addition, future experiments will probe intermediate and high mass regions. Nevertheless, in absence of signals, it will not be possible to rule out these two regions. Notice the proximity of the region where the coherent neutrino scattering is an irreducible background.

With this one sees that the Inert Higgs Doublet Model gives a still viable DM candidate, which will most likely be tested by direct DM detection experiments.

### Acknowledgments

We thank conversations with Drs. Germán Gómez, Nicolás Viaux, and Edson Carquín. M.A.D. was partly supported by Fondecyt 1141190. B.K. was partly supported by Fondecyt 1120360. S.U-Q. was partly supported by postgraduate CONICYT grant. The work of all of us was also partly financed by CONICYT grant ANILLO ACT-1102.

- 
- [1] D. Clowe, M. Bradac, A. H. Gonzalez, M. Markevitch, S. W. Randall, C. Jones and D. Zaritsky, *Astrophys. J.* **648**, L109 (2006) [astro-ph/0608407].
  - [2] P. A. R. Ade *et al.* [Planck Collaboration], *Astron. Astrophys.* **571**, A1 (2014) [arXiv:1303.5062 [astro-ph.CO]].
  - [3] V. C. Rubin, N. Thonnard and W. K. Ford, Jr., *Astrophys. J.* **238**, 471 (1980).
  - [4] M. Markevitch *et al.*, *Astrophys. J.* **606**, 819 (2004) [astro-ph/0309303].
  - [5] W. J. Percival, S. Cole, D. J. Eisenstein, R. C. Nichol, J. A. Peacock, A. C. Pope and A. S. Szalay, *Mon. Not. Roy. Astron. Soc.* **381**, 1053 (2007) [arXiv:0705.3323 [astro-ph]].
  - [6] C. J. Copi, D. N. Schramm and M. S. Turner, *Science* **267**, 192 (1995) [astro-ph/9407006].
  - [7] N. Blinov, J. Kozaczuk, D. E. Morrissey and A. de la Puente, arXiv:1510.08069 [hep-ph].
  - [8] N. Khan and S. Rakshit, *Phys. Rev. D* **92**, 055006 (2015) [arXiv:1503.03085 [hep-ph]].
  - [9] G. Belanger, B. Dumont, A. Goudelis, B. Herrmann, S. Kraml and D. Sengupta, *Phys. Rev. D* **91**, no. 11, 115011 (2015) [arXiv:1503.07367 [hep-ph]].
  - [10] N. G. Deshpande and E. Ma, *Phys. Rev. D* **18**, 2574 (1978).
  - [11] I. F. Ginzburg, K. A. Kanishev, M. Krawczyk and D. Sokolowska, *Phys. Rev. D* **82**, 123533 (2010) [arXiv:1009.4593 [hep-ph]].
  - [12] L. Lopez Honorez and C. E. Yaguna, *JHEP* **1009**, 046 (2010) [arXiv:1003.3125 [hep-ph]].
  - [13] A. Arhrib, Y. L. S. Tsai, Q. Yuan and T. C. Yuan, *JCAP* **1406**, 030 (2014) [arXiv:1310.0358 [hep-ph]].
  - [14] G. Aad *et al.* [ATLAS Collaboration], *Phys. Lett. B* **716**, 1 (2012) [arXiv:1207.7214 [hep-ex]].
  - [15] S. Chatrchyan *et al.* [CMS Collaboration], *JHEP* **1306**, 081 (2013) [arXiv:1303.4571 [hep-ex]].
  - [16] M. Gustafsson, *PoS CHARGED 2010*, 030 (2010) [arXiv:1106.1719 [hep-ph]].
  - [17] E. C. F. S. Fortes, A. C. B. Machado, J. Montao and V. Pleitez, *J. Phys. G* **42**, no. 11, 115001 (2015) [arXiv:1408.0780 [hep-ph]].

- [18] M. Krawczyk, D. Sokolowska, P. Swaczyna and B. Swiezewska, *Acta Phys. Polon. B* **44**, no. 11, 2163 (2013) [arXiv:1309.7880 [hep-ph]].
- [19] R. Barbieri, L. J. Hall and V. S. Rychkov, *Phys. Rev. D* **74**, 015007 (2006) [hep-ph/0603188].
- [20] A. Djouadi, *Phys. Rept.* **457**, 1 (2008) [hep-ph/0503172].
- [21] A. Arhrib, R. Benbrik and N. Gaur, *Phys. Rev. D* **85**, 095021 (2012) [arXiv:1201.2644 [hep-ph]].
- [22] M. E. Peskin and T. Takeuchi, *Phys. Rev. D* **46**, 381 (1992).
- [23] B. Swiezewska, *Phys. Rev. D* **88**, no. 5, 055027 (2013) [erratum: *Phys. Rev. D* **88**, no. 11, 119903 (2013)] [arXiv:1209.5725 [hep-ph]].
- [24] M. Baak *et al.* [Gfitter Group Collaboration], *Eur. Phys. J. C* **74**, 3046 (2014) [arXiv:1407.3792 [hep-ph]].
- [25] E. Lundstrom, M. Gustafsson and J. Edsjo, *Phys. Rev. D* **79**, 035013 (2009) [arXiv:0810.3924 [hep-ph]].
- [26] Q. H. Cao, E. Ma and G. Rajasekaran, *Phys. Rev. D* **76**, 095011 (2007) [arXiv:0708.2939 [hep-ph]].
- [27] A. Pierce and J. Thaler, *JHEP* **0708**, 026 (2007) [hep-ph/0703056 [HEP-PH]].
- [28] G. Belanger, F. Boudjema and A. Pukhov, arXiv:1402.0787 [hep-ph].
- [29] C. L. Bennett *et al.* [WMAP Collaboration], *Astrophys. J. Suppl.* **208**, 20 (2013) [arXiv:1212.5225 [astro-ph.CO]].
- [30] P. A. R. Ade *et al.* [Planck Collaboration], arXiv:1502.01589 [astro-ph.CO].
- [31] G. Bohm and G. Zech [Verlag Deutsches Elektronen-Synchrotron], “Introduction to Statistics and Data Analysis for Physicists.”
- [32] L. Lopez Honorez and C. E. Yaguna, *JCAP* **1101**, 002 (2011) [arXiv:1011.1411 [hep-ph]].
- [33] M. Cirelli, N. Fornengo and A. Strumia, *Nucl. Phys. B* **753**, 178 (2006) [hep-ph/0512090].
- [34] A. Goudelis, B. Herrmann and O. Stål, *JHEP* **1309**, 106 (2013) [arXiv:1303.3010 [hep-ph]].
- [35] J. F. Gunion, H. E. Haber, G. L. Kane and S. Dawson, *Front. Phys.* **80**, 1 (2000).
- [36] ATLAS collaboration, ATLAS-CONF-2015-081.
- [37] CMS Collaboration, CMS-PAS-EXO-15-004.
- [38] M. Krawczyk, D. Sokolowska, P. Swaczyna and B. Swiezewska, *JHEP* **1309**, 055 (2013) [arXiv:1305.6266 [hep-ph]].
- [39] A. Djouadi, J. Kalinowski and M. Spira, *Comput. Phys. Commun.* **108**, 56 (1998) [hep-ph/9704448].
- [40] G. Aad *et al.* [ATLAS Collaboration], *Phys. Rev. D* **90**, no. 11, 112015 (2014) [arXiv:1408.7084 [hep-ex]].
- [41] V. Khachatryan *et al.* [CMS Collaboration], *Eur. Phys. J. C* **75**, no. 5, 212 (2015) [arXiv:1412.8662 [hep-ex]].
- [42] A. Ilnicka, M. Krawczyk and T. Robens, arXiv:1508.01671 [hep-ph].
- [43] G. Aad *et al.* [ATLAS Collaboration], *Phys. Lett. B* **732**, 8 (2014) [arXiv:1402.3051 [hep-ex]].
- [44] S. Chatrchyan *et al.* [CMS Collaboration], *Phys. Lett. B* **726**, 587 (2013) [arXiv:1307.5515 [hep-ex]].
- [45] C. S. Chen, C. Q. Geng, D. Huang and L. H. Tsai, *Phys. Rev. D* **87**, 075019 (2013) [arXiv:1301.4694 [hep-ph]].
- [46] B. Swiezewska and M. Krawczyk, *Phys. Rev. D* **88**, no. 3, 035019 (2013) [arXiv:1212.4100 [hep-ph]].
- [47] G. Aad *et al.* [ATLAS Collaboration], arXiv:1508.07869 [hep-ex].
- [48] S. Chatrchyan *et al.* [CMS Collaboration], *Eur. Phys. J. C* **74**, 2980 (2014) [arXiv:1404.1344 [hep-ex]].

- [49] K. A. Olive *et al.* [Particle Data Group Collaboration], *Chin. Phys. C* **38**, 090001 (2014).
- [50] T. Hambye, F.-S. Ling, L. Lopez Honorez and J. Rocher, *JHEP* **0907**, 090 (2009) [erratum: *JHEP* **1005**, 066 (2010)] [arXiv:0903.4010 [hep-ph]].
- [51] A. Djouadi, O. Lebedev, Y. Mambrini and J. Quevillon, *Phys. Lett. B* **709**, 65 (2012) [arXiv:1112.3299 [hep-ph]].
- [52] S. Kanemura, S. Matsumoto, T. Nabeshima and N. Okada, *Phys. Rev. D* **82**, 055026 (2010) [arXiv:1005.5651 [hep-ph]].
- [53] J. M. Alarcon, L. S. Geng, J. Martin Camalich and J. A. Oller, *Phys. Lett. B* **730**, 342 (2014) [arXiv:1209.2870 [hep-ph]].
- [54] R. D. Young and A. W. Thomas, *Phys. Rev. D* **81**, 014503 (2010) [arXiv:0901.3310 [hep-lat]].
- [55] D. Toussaint *et al.* [MILC Collaboration], *Phys. Rev. Lett.* **103**, 122002 (2009) [arXiv:0905.2432 [hep-lat]].
- [56] D. S. Akerib *et al.* [LUX Collaboration], *Phys. Rev. Lett.* **112**, 091303 (2014) [arXiv:1310.8214 [astro-ph.CO]].
- [57] R. Agnese *et al.* [SuperCDMS Collaboration], *Phys. Rev. Lett.* **112**, no. 4, 041302 (2014) [arXiv:1309.3259 [physics.ins-det]].
- [58] R. Agnese *et al.* [SuperCDMS Collaboration], *Phys. Rev. Lett.* **112**, no. 24, 241302 (2014) [arXiv:1402.7137 [hep-ex]].
- [59] R. Gaitskell *et al.* [Dark Matter Tools Workgroup, UCB], `dmttools.berkeley.edu`.
- [60] J. Billard, L. Strigari and E. Figueroa-Feliciano, *Phys. Rev. D* **89**, no. 2, 023524 (2014) [arXiv:1307.5458 [hep-ph]].